Monte Carlo simulation of small hydrate clusters of NO_2^-

Ajit Banerjee, Ron Shepard, and Jack Simons[a)]

Department of Chemistry, University of Utah, Salt Lake City, Utah 84112
(Received 21 January 1980; accepted 28 April 1980)

The ground-state Hartree–Fock (HF) potential for the NO_2^-:H_2O dimer has been computed for 102 different intermolecular geometrical configurations and has been expressed in a computationally convenient analytical form. The main conclusion drawn from these calculations is that the ion–solvent attraction is mainly electrostatic for intermolecular distances between 6.0 and 7.0 bohr (N-to-O distance). Keeping the dipole vector of the H_2O molecule oriented toward the NO_2^- ion yields energetically favorable conformations. Rotations of the H_2O molecule which do not change the dipole orientation of the H_2O have been found to have small barriers ($\sim$4 kcal/mole), whereas those that destroy proper dipole alignment encounter large ($\sim$30 kcal/mole) barriers. The use of such ion–H_2O intermolecular potentials together with the H_2O:H_2O pair potential of Clementi permits Monte Carlo techniques to be used to examine the nature of the inner hydration shells of NO_2^-. The results of Monte Carlo simulations of $NO_2^-(H_2O)_n$ $1 \leq n \leq 15$ are discussed in some detail.

I. INTRODUCTION

The solvation phenomenon has been a subject of long chemical interest in gas-phase kinetics,[1–3] thermodynamics of ion clustering processes,[2] spectroscopic studies,[3] and many biological problems.[3] A comprehensive multilevel understanding of the solvation process would be extremely valuable in deciphering the rapidly accumulating experimental data and in pointing out fruitful directions for further research. One would like to know answers to questions regarding the structure, energetics, and dynamics of the ground and excited electronic states of solvated molecules and ions.

Our pursuits toward understanding the solvation process began with an analysis of the electronic spectroscopy[4] and mobility[5] of solvated molecules and ions in pure and mixed solvents, within a statistical mechanical framework expressed in terms of correlation functions. The dynamical properties of a molecule or ion in equilibrium with a surrounding medium were expressed in terms of a specific correlation function of the solute–solvent system (e.g., the electric dipole correlation function was related to the optical absorption spectrum). The time dynamics contained in the such correlation functions involves the motion of the solute and the solvent. In our approach, one transforms this problem to one of studying the property of a single "dressed" molecule which feels static solvation effects plus the presence of a time-dependent external field which contains fluctuations in the solute–solvent interactions. The predictive utilization of this theory requires knowledge of the complicated solute–solvent interactions as well as knowledge of the electronic–vibrational energy levels of the solvated species. One of the aims of the present endeavor is to provide information about such solute–solvent interactions for the prototype NO_2^- (aq) system.

The present series of articles, of which the present manuscript is the first, comprises a study of the structure and electronic spectroscopy of solvated anions based upon the use of *ab initio* quantum chemical methods in conjunction with Monte Carlo simulation techniques. Specifically, we want to know about the equilibrium intermolecular geometries (or most probable geometries at finite temperatures) in the ground electronic state of the solvated molecule as well as the energies involved in distorting the solute–solvent system away from these favored geometries. This is the primary question addressed in the research reported here.

Possible differential stabilization of either the ground or excited electronic state of the anion must also be studied because such efforts give rise to spectroscopic solvent shifts. Knowledge of the geometries of the complex which are thermally accessible at a given temperature yield insight into the inhomogeneous broadening of such electronic spectral lines. This investigation of effects of solvation on excited electronic states represents the subject of our second paper on this subject.

The most commonly employed approaches to the solvation problem can be separated into two categories. The cavity model for solvated electrons in polar solvents dates back to the early pioneering works of Ogg,[6] Lipscomb,[7] Stairs,[8] and Jortner,[9] from which a host of more elaborate models were developed.[10–13] In these models the electron is assumed to be localized in a "cavity" at some point in space and to have an electronic wave function which decreases exponentially with distance away from this point. The potential energy of the cavity is assumed to be due to the dipolar orientation of the polar molecules toward the cavity center. Within the class of cavity models, the simple cluster type[10] models treat only the first solvation layer. Continuum models[11] assume the cavity to be surrounded by a continuum dielectric medium. The semicontinuum[12,13] models combine these two extremes by using a cavity surrounded by a cluster of solvent molecules embedded in a polarizable dielectric continuum. These models differ in the degree of sophistication with which they treat the solvent molecules of the first solvation layer (point charge, *ab initio*, etc.) and the dielectric continuum. The most sophisticated among such treatments are the calculations of Newton[13] on solvated electrons in H_2O and NH_3, in which the cavity size and the number of molecules in the first solvation layer are determined by the *ab initio*

[a)]Camille and Henry Dreyfus Teacher–Scolar, David P. Gardner Research Fellow, John Simon Guggenheim Fellow.

 0021-9606/80/161814-13$01.00

self-consistent-field (SCF) approach. Such cluster models have had relatively good success in describing the behavior of trapped electrons in polar solvents although the conformational variations of the solvent cannot easily be accounted for and, hence, the spectroscopic predictions of the band shape are usually only qualitatively correct.

The second category of approaches to solvation are based on more traditional molecular quantum chemical techniques. Examples are contained in the works of Clementi,[14] the Pullmans,[15] and others.[16–19] In the supermolecule approach[15] used by the Pullmans, the solvent molecules are gradually built up around the solute via SCF calculations including reorganization until the first solvation layer is completed. This approach, though straightforward and accurate, neglects the polarization effects due to the second solvation layer and is limited by the size of the basis sets which are practical to use. Newton and Ehrenson[13] and Noell and Morokuma[19] have shown that effects beyond the first solvation layer are important for describing the behavior of solvated electrons in H_2O and NH_3. In addition, weakly bonded systems such as solvated hydrocarbons or biomolecules may require of the order of 50 solvent molecules to complete the first solvation layer, in which case a complete *ab initio* calculation is likely to be impractical.

Clementi and others have extensively used a technique which utilizes intermolecular pair potentials to simulate the full potential of a solute with N solvent molecules. The basic idea is to first perform *ab initio* [SCF or configuration interaction (CI)] calculations on the solute–solvent and solvent–solvent dimer systems. Analytic functions of the interparticle coordinates are then fit to the computed points on the energy surfaces which are subsequently used (within the pairwise additive potential approximation) to calculate potentials for any number of solvent molecules around the solute. This technique has been very successfully combined with Monte Carlo dynamics simulation to extract equilibrium averaged structural and thermodynamic properties of molecules, ions, and macromolecules in solution. Thus far, this procedure has only been applied to ground electronic states, although we are currently in the process of extending the work presented here to the $(n\pi^*)$ state of NO_2^-.

The procedure that we chose to adopt is essentially the pair potential approach of Clementi. Because we are interested in the effects of solvation on electronic spectra, we must compute the low-lying $(n\pi^*)$ excited state of the $NO_2^-(H_2O)$ pair as well as the ground state energy which determines the equilibrium properties of the system. The effect of nonpairwise additive forces have been estimated by Clementi to alter the ground state energetics of such strongly interacting systems having long-range forces by approximately 10%. These effects should be even smaller for the two-state energy differences. Quite frankly, though, we simply can not afford to carry out *ab initio* calculations on higher clusters. As a result, we must limit our treatment to the pairwise additive approximation. In the present article of this series, we devote our attention primarily to the two-body solute–solvent interaction potential for the ground state of $NO_2^-:H_2O$ and the Monte Carlo simulation of the solvent hydration shell structure arising from this ground-state potential. The excited states, which require configuration interaction will be treated in more detail in a subsequent article, as will the Monte Carlo simulation of the inhomogeneous broadening effects.

II. ATOMIC BASIS SETS

The atomic orbital basis sets employed for NO_2^- are augmentations of Dunning's $[4s, 2p]$ contraction[20] of Huzinaga's $[9s, 5p]$ Gaussian bases[21] for nitrogen and oxygen. Diffuse s and p functions for nitrogen and a diffuse p function for oxygen were added to complete the basis. The SCF-level ground state $(X\,^1A_1)$ energy of the NO_2^- anion was minimized at the experimental ground state geometry ($\theta_{ONO} = 115.4°$, $R_{NO} = 2.3356$ bohrs) to determine the optimum orbital exponents for these diffuse functions. It is well known that the addition of such diffuse functions is necessary for describing the charge density of negative ions.[22] It is probably particularly important in the present case since we wish to treat the spectroscopy of NO_2^- which involves excitations of the loosely bound "extra" electron. The minimum energy geometry of NO_2^- for our basis (Table I) ($\theta_{ONO} = 117.0°$, $R_{NO} = 2.39$ bohr) yielded an SCF energy of $E_{SCF}(X\,^1A_1) = -204.044\,510$ hartrees. This SCF energy is comparable to the results of Bonacorsi *et al.*[23] (−203.9859 hartrees) and of Benioff[24] (−204.0487 hartrees).

For describing the H_2O molecule, we used a slightly uncontracted version of the 4-31G basis of Ditchfield *et al.*[25] which is also shown in Table I. The exponents we again optimized at the ground state $(^1A_1)$ experimental geometry ($\theta_{HOH} = 104.45°$, $R_{OH} = 1.8111$ bohrs). The minimum energy SCF$(^1A_1) = -75.910\,516$ hartrees, which obtains at $\theta_{HOH} = 111.3°$ and $R_{OH} = 1.790$ bohrs, is comparable to the energy of Newton and Ehrenson (−75.9086 hartrees) who used the 4-31G basis.[13] By comparing the results of the 4-31G basis with those of larger bases which include both more core orbtials and polarization functions ($2p$ functions for hydrogen, and $3d$ functions for oxygen), Newton concludes that the 4-31G basis has sufficient flexibility for describing the ion–water, and water–water potential energy surfaces even though the dipole moment of H_2O obtained in this basis is substantially larger than the gas-phase dipole of H_2O. The absolute errors (0.1 hartrees for H_2O) in the 4-31G basis' SCF energy have been found to result mainly from errors in the atomic core energy which is caused by using fewer contracted basis functions. For the reasons put forth by Newton,[13] we believe that the somewhat uncontracted version of the water molecule 4-31G basis set given in Table I should give an adequate description of the $NO_2^-(H_2O)$ potential energy surface.

III. METHODS FOR OBTAINING THE $NO_2^-:H_2O$ INTERACTION

A. Assumptions and restrictions on the Geometrical degrees of freedom

The following assumptions have been made in the calculation of the $NO_2^-:H_2O$ intermolecular potential pre-

TABLE I. Basis sets.

NO_2^- basis set		
Center	Type	
N	s	5909.44(0.002004), 887.451(0.015310), 204.749(0.074293), 59.8376(0.253364), 19.9981(0.600576), 2.6860(0.245111),
	s	7.1927(1.0)
	s	0.7(1.0)
	s	0.2133(1.0)
	s	0.0854(1.0)
	$p(x,y,z)$	26.7860(0.018257), 5.9564(0.116407), 1.7074(0.390111), 0.5314(0.637221)
	$p(x,y,z)$	0.1654(1.0)
	$p(x,y,z)$	0.0413(1.0)
O	S	7816.54(0.002031), 1175.82(0.015436), 273.18(0.073771) 81.1696(0.247606), 27.1836(0.611832), 3.4136(0.241205)
	S	9.5322(1.0) 0.9398(1.0) 0.2846(1.0)
	$p(x,y,z)$	35.1832(0.019580), 7.9040(0.124189), 2.3051(0.394727), 0.1771(0.627375)
	$p(x,y,z)$	0.2137(1.0)
	$p(x,y,z)$	0.0527(1.0)
H_2O basis set		
O	s	883.2729(0.0175506), 133.1293(0.1228292), 29.90641(0.4348836) 7.978677(0.5600108)
	s	15.86894(0.113401), 3.704106(0.1772865)
	s	15.86894(0.113401), 3.704106(0.1772865)
	s	1.04(1.0)
	s	0.2781159(1.0)
	$p(x,y,z)$	15.86894(0.0685453), 3.704106(0.3312254), 1.049455(0.7346079)
	$p(x,y,z)$	0.2781159(1.0)
H	s	20.98016(0.0334946), 3.164637(0.234727), 0.7169808(0.813573)
	s	0.1905456(1.0)

sented here: 1) The Hartree–Fock model is assumed to provide a sufficiently accurate picture of the interactions for the ground electronic state of the dimer. This amounts to assuming that the electronic correlation energy of the ground state supermolecule does not differ greatly from that of its constiuent parts. Because $NO_2^-:H_2O$ is a closed-shell species without strong intermolecular chemical bonding, it is natural to assume that correlation effects are not likely to grossly alter the HF-level description of the statistical properties of the ground state of this dimer. However, spectroscopic properties, which are sensitive to the intraionic correlation energy of NO_2^- requires correlation effects to be treated. In the next publication of this series we present results of such correlated calculations for the ground and $(n\pi^*)$ excited states of $NO_2^-:H_2O$. Because HF calculations are performed for each $NO_2^-:H_2O$ intermolecular geometry, polarization effects are taken into consideration. 2) We further assume that variations in the internal degrees of freedom of the fragments (the bond angle and bond lengths of NO_2^- and H_2O) are of relatively minor importance in determining the structure of the supermolecule. Hence we freeze these geometrical variables at their isolated-species equilibrium values. In support, of this action, we mention that our earlier study[4] of NO_2^- and $NO_2^-:H_2O$ show that the change in NO_2^- bond angle is approximately 0.1 degrees even for dimer conformations which involve strong hydrogen bonding to the nitrite anion's oxygen atoms. Of course, we must return eventually to consider, as in Ref. 4, the role played by the Franck–Condon progression involving the ν_2 bending mode of NO_2^- in determining the $n\pi^*$ absorption line shape. A primary reason for making the above geometrical approximation is the reduction in the number of geometrical degrees of freedom and hence computational effort which results. For the specific case under consideration, $(NO_2^-:H_2O)$, there are 18 total degrees of freedom. Deleting the six internal degrees of

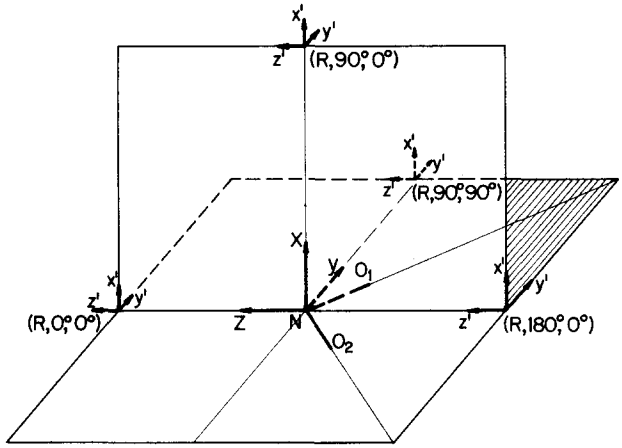

FIG. 1. Coordinate system for describing the $NO_2^-:H_2O$ dimer The NO_2^- is fixed in the YZ plane with the coordinate origin at the N atom. (R,θ,ρ) is used to describe the position of the O atom of the H_2O; the angles α, β describe the orientation of its dipole vector and γ shows the rotation angle around this dipole vector.

freedom of the dimer, we are left with six degrees of freedom to be considered. The interaction potential between NO_2^- and H_2O would involve three coordinates to describe the relative position of the H_2O molecule's center-of-mass and three degrees of freedom describing the orientation of the H_2O. Even with these restrictions, one needs to compute a large number of SCF energy values for the calculation of the $NO_2^-:H_2O$ system. In performing the SCF calculations reported here, a set of spherical polar coordinates R, θ, ϕ are chosen to describe the position of the O atom of the H_2O molecule. To describe the orientation of the H_2O molecule, we use the angles α and β of the dipole moment vector of the H_2O molecule and an angle γ involving the rotation of H_2O around its dipole vector (see Fig. 1).

B. Sampling the geometrical conformations

Faced with the problem that such a large number of conformation points are required to describe the potential surface of the dimer, one needs systematic procedures to sample the more relevant parts of the surface. Because of the inherent symmetry of the problem, $E(R, \theta, \phi, \ldots) = E(R, 2\pi - \theta, \ldots)$ and $E(R, \theta, \phi, \ldots) = E(R, \theta, \pi/2 + \phi, \ldots)$, we need only consider the quadrant $0 < \theta < \pi$ and $0 \leq \phi \leq \pi/2$. There are at least two additional guidelines which can be used to facilitate sampling of the geometrical conformations. The ground-state energy surface with an H_2O molecule in any geometrical conformation labeled (i) for which the dimer $NO_2^-:H_2O$ energy is E_i will have a relative thermal probability for $\exp(-\Delta E_i/KT)$, where $\Delta E_i = E_i - E_0$ and E_0 is the minimum energy in the $NO_2^-:H_2O$ potential hypersurface. Thus, it is not probable that we will have to consider conformations which lie above E_0 by an amount of the order of 10 KT, although one must, of course, also take into account the water–water interactions in determining the most important configurations of larger $NO_2^-:(H_2O)_n$ clusters. Because of the Boltzmann weighting, we are more interested in accurately determining the potential surface in the neighborhood of the energy minimum (E_0) (or low-energy local minima) than at points which are energetically far away. Therefore, the density of computed (SCF) points and their weights were determined by the Boltzmann factor, $\exp(-\Delta E_i/KT)$, which has the effect of restricting regions of space and weighing the more probable conformations heavier than the less probable ones. In order to carry out an accurate, yet efficient, implementation of the above procedure, one needs to have a reasonably accurate idea about the most likely low energy conformations as well as the energy increments which accompany variations in each degree of freedom in the neighborhoods of these conformations. To accomplish such an initial probe of the hypersurface, we performed calculations within a very simple point charge model. It was not the purpose of these calculations to obtain accurate values for the conformational energies ΔE_i but rather to attempt to identify those conformations which are likely to have relatively low ΔE_i values. These point-charge energy estimates were undertaken only after we noticed that such a model seemed to be capable of reproducing the energy variations which accompanied angle variations in our earliest SCF computations.

The point-charge energy estimates involve calculating the interaction energy of the anion–solvent system using point charges to simulate the charge distributions of the isolated systems. A rather sophisticated point charge model which preserves the total charge and dipole moment has been developed by Hall.[26] In our case, the electrostatic potentials around NO_2^- and H_2O were approximated by replacing each atomic center by an appropriate charge obtained by a population analysis which preserves total charge and dipole moment. To include the repulsive potential energy terms which such a point-charge model (PCM) ignores, we have chosen to scale the simple point-charge model as follows:

$$E_{PC}^{Scaled}(R,\theta,\phi,\alpha,\beta,\gamma) = E_{PC}(R,\theta,\phi,\alpha,\beta,\gamma) + [E_{SCF}(R,180°,0,0,0,0) - E_{PC}(R,180°,0,0,0,0)]$$

where $E_{SCF}(R,180°,0,0,0,0)$ is the SCF energy computed for the most favored "approach" of the H_2O molecule shown in Fig. 2(a) and $E_{PC}(R,180°,0,0,0)$ is the PCM energy at this same conformation. In the following section we compare some of PCM results with those of our *ab initio* SCF calculations to justify the use of the model in predicting the most likely thermally accessible regions of configuration space. After thus using this model to "guess" favorable conformations from among *more than one million conformations* considered, we have performed SCF calculations at more than 100 conformational points of the $NO_2^-:H_2O$ dimer.

IV. ANALYSIS OF THE $NO_2^-:H_2O$ INTERMOLECULAR POTENTIAL

A. Electron distribution and bonding

Before moving on to discuss the results of the $NO_2^-:H_2O$ dimer potential surface calculation, it is instructive to consider the nature of the electron distributions of the fragments NO_2^- and H_2O as well as the strengths of the couplings between $H_2O:H_2O$ and $NO_2^-:H_2O$. The potential energy curve arising from

variations of R for the geometrical arrangement depicted in Fig. 2(a) is shown in Fig. 3(a). The binding energy for this lowest energy conformation is approximately 17 kcal/mole, which is nearly three times the $H_2O:H_2O$ hydrogen bond attraction.[14] Moreover, at the minimum of this potential energy curve ($R=6.5$ bohr) the distance between the O atoms of NO_2^- and the H atoms of H_2O is 2.2 Å which is comparable to the hydrogen-bond length in $H_2O:H_2O$ (2.1 Å).

Another observation which should be made here is that the orbital couplings between NO_2^- and H_2O are very small for the thermally populated regions of the conformation space studied here ($\Delta E \lesssim 10\ KT$); although they are indeed polarized or distorted (as is expected) the orbitals of $NO_2^-:H_2O$ can clearly be identified as belonging either to NO_2^- or H_2O for the thermally accessible conformations. At other conformations, especially at small R values, the orbital couplings increase substantially.

B. Energy surfaces and rotational barriers

In this subsection we describe portions of the $NO_2^-:H_2O$ energy surface for the interactions of the nitrite ion fixed at the origin (the N atom at the origin, O atoms in yz plane) with an H_2O molecule at various geometrical conformations. For reference, the coordinates ($R, \theta, \phi, 0, 0, 0$) imply that the O nucleus of the H_2O molecule is at (R, θ, ϕ) and the H nuclei are the $y'z'$ plane (the H_2O body-fixed $x'y'z'$ axes are parallel to the xyz axis with their origin on the O nucleus). The z' axis bisects the HOH angle. The rotations α, β involve motion about the Y' and X' axes and hence determine the orientation of the dipole vector of H_2O. γ is the rotation angle around the dipole vector of H_2O.

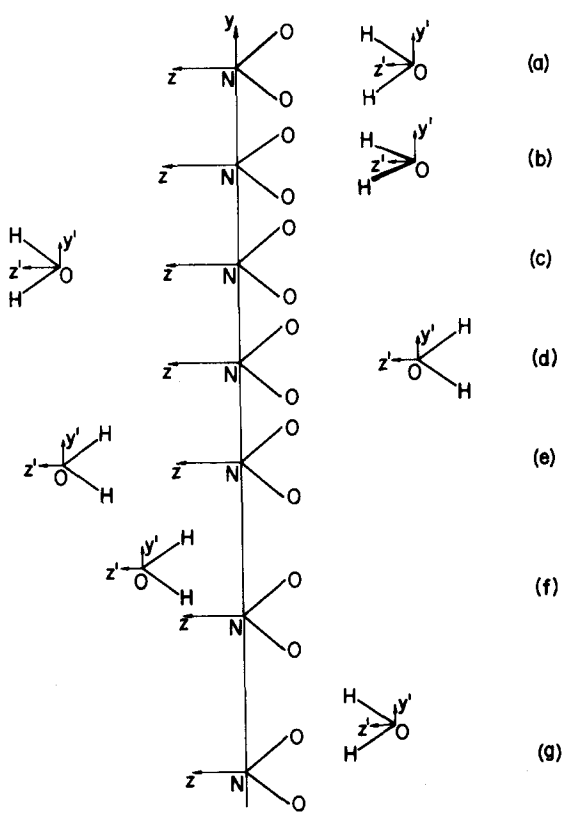

FIG. 2. Selected conformations of the $NO_2^-:H_2O$ dimer. The potential energy curves corresponding to variuus geometry variations starting from these initial conformations are shown in Figs. 3–7. (a) (R, 180°, 0, 0, 0, 0); (b) (R, 180°, 0, 0, 0, 90°); (c) (R, 0, 0, 0, 0, 0); (d) (R, 180°, 0, 180°, 0, 0); (e) (R, 0, 0, 180°, 0, 0); (f) (6.5, 60, 90°, 180°, 0, 0); (g) (6.5, 120°, 90°, 0, 0, 0).

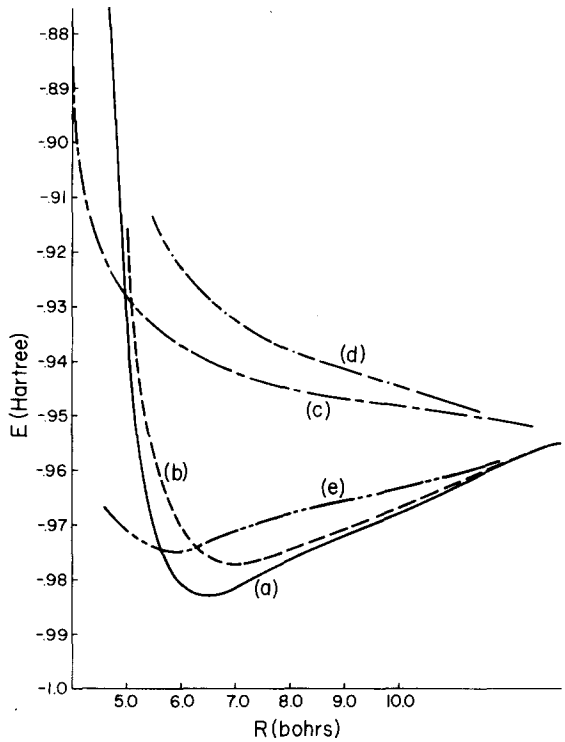

FIG. 3. Potential energy curves as a function of R (in bohrs) for various conformations shown in Fig. 2. (a) (R, 180°, 0, 0, 0, 0); (b) (R, 180°, 0, 0, 0, 90°), (c) (R, 0, 0, 0, 0, 0); (d) (R, 180°, 0, 180°, 0, 0), (e) (R, 0, 0, 180°, 0, 0).

As stated earlier, the scaled PCM was used as an *initial probe* to sample for energetically favorable conformations. Based upon the results of this model and our nearly 100 SCF calculations, we conclude that the energetically favorable conformations of the H_2O molecule (within ~12 KT) lie within an annular sphere ($6.0 \leq R \leq 7.5$ bohr) in R space with the hydrogen atoms of the H_2O aligned toward the oxygen or nitrogen atoms of NO_2^-. Further details of these findings are discussed below.

R dependence

Figure 2 shows various conformations of the H_2O molecule for which the potential energy curves for R variation are shown in Fig. 3. The conformation of Fig. 2(b): (R, 180°, 0, 0, 0, 90°) is obtained from that of 2(a) by a 90° rotation (in γ) about the dipole vector of the H_2O molecule. This conformation has an energy minimum at $R=6.8$ bohrs (Fig. 3). Based upon qualitative arguments, (including PCM results), conformation 2(b) was thought to be more favorable than 2(a). However, our SCF results show that the electronic energy of 2(b) is 5 kcal/mole higher than that of 2(a). The energetics of

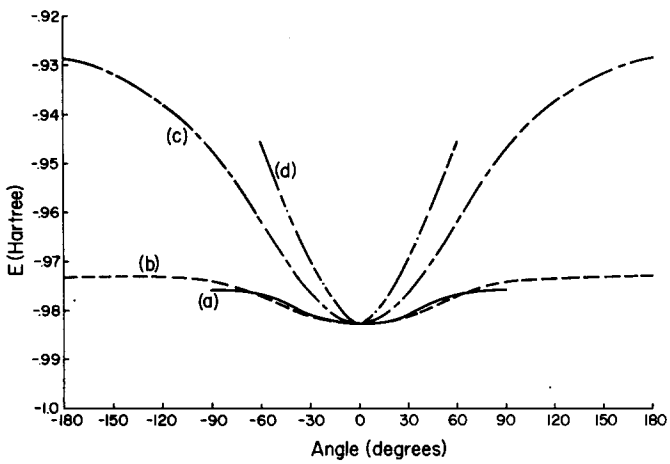

FIG. 4. Rotational barriers around the most favored conformation (6.5, 180°, 0, 0, 0, 0); (a) (6.5, 180°, 0, 0, 0, γ); (b) (6.5, θ, 0, $\alpha(\theta)$, 0, 0), (c) (6.5, 180°, 0, α, 0, 0), (d) (6.5, θ, 90°, 0, 0, 0). See text for explanation of $\alpha(\beta)$.

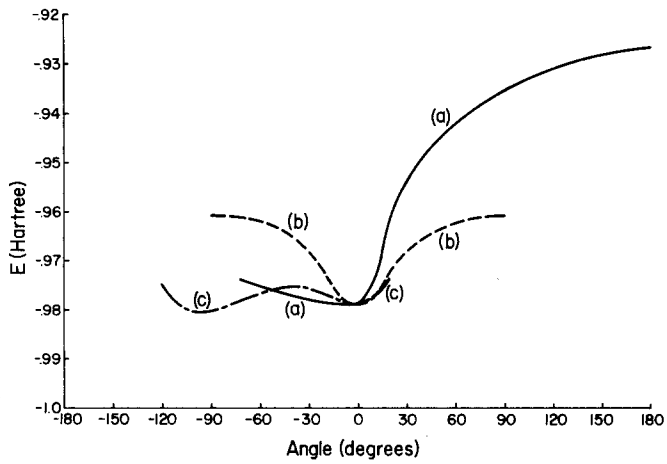

FIG. 6. Rotational barriers around the conformation (6.5, 70°, 90°, 180°, 0, 0); (a) (6.4, 70°, θ, 90°, 180°, 0, 0), (b) (6.4, 70°, 90° ϕ, 180°, 0, 0); (c) rotation around the x' axis (6.4, 70°, 90°, 180°, β, 0).

conformations 2(c) (R, 0, 0, 0, 0, 0) and 2(d) (R, 180°, 0, 180°, 0, 0) can be understood in terms of the PCM (which is compatible with the SCF description). These conformations are related to conformations 2(e): (R, 0, 0, 180°, 0, 0), and 2(a): (R, 180°, 0, 180°, 0, 0), respectively, by a rotation of the H_2O molecule which moves the H atoms of the H_2O molecule away from the O atoms of NO_2^- and exposes the dominant repulsive interaction between the lone-pairs of the H_2O O atom and the O and N atoms of NO_2^-.

The general conclusions to be drawn from these SCF calculations are: 1) that the interaction between the NO_2^- and H_2O in the thermally populated region is mainly electrostatic, 2) there is small distortion of the unperturbed orbitals of the individual species; 3) energetically favorable conformations lie within an annulus of 6.2 to 7.0 bohrs, 4) conformations which align the H atoms of the water molecule toward the N or O atoms of the NO_2^- are energetically more favorable, 5) the strength of the $NO_2^-:H_2O$ iteration (~17 kcal/mole) is larger than that of the $H_2O:H_2O$ attraction (~5 kcal/mole), and, on a scale of KT (~0.6 kcal/mole), the $NO_2^-(H_2O)$ potential surface is *quite anisotropic* even when the H_2O molecule is properly aligned, 6) the attractive regions of configuration space near $\theta = 180°$ are approximately 5 kcal/mole lower in energy than those near $\theta = 0°$. It should also be mentioned that for geometries such as one shown in Fig. 2(a), $R = 6.5$ a.u. corresponds to a distance of 2.2 Å between the H atoms of H_2O and the O atoms of NO_2^-. This distance (R_{OH}) is comparable to that of normal hydrogen bonds between neutral species ($R_{OH} \approx 2.1$ Å).

Rotational barriers

Figures 4–7 show the barriers to various rotations in the neighborhoods of a few representative energetically favorable conformations. Figure 4 displays the barriers around the most favorable geometry: (6.5, 180°, 0, 0, 0, 0) shown in Fig. 2(a). Rotation of the H_2O around its dipole (γ motion) [Fig. 4(a)] has the lowest barrier (4.4 kcal/mole) of any rotation. The next "easiest" rotation is the θ rotation of the entire H_2O molecule (around the y axis), with the constraint that the H_2O dipole points

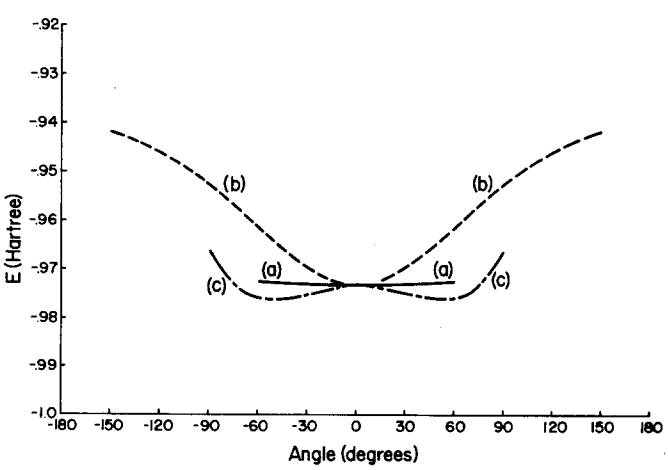

FIG. 5. Rotational barriers around to conformation (6.5, 0, 90°, 180°, 0, 0). (a) (6.5, 0, 90: 180°, 0, γ), (b) (6.5, 0, 90°, 180°, α, 0, 0) (c) (6, 5, θ, 90°, 0, 0, 0).

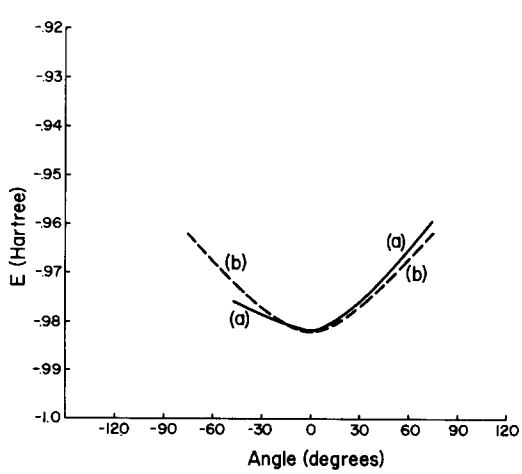

FIG. 7. Rotational barriers around the conformation (6.2, 150°, 0, 320°, 0, 0); (a) (6.2, 150°, 0, 320° α, 0, 0), (b) (6.2, 150°, ϕ, 320°, 0, 0).

toward the O atoms of NO_2^-: $(6.5, \theta, 0, \alpha(\theta), 0, 0)$, (e.g., at $\theta = 90°$, $\alpha = 259.12°$). This rotation [Fig. 4(b)] also has a small barrier of 6.5 kcal/mole. The above two rotations are seen to keep the dipole (H atoms) of the H_2O aligned toward the O atoms of NO_2^-. The rotations which violate this rule [Fig. 4(c), 4(d)] show much larger barriers as typified by the θ rotations for $\phi = 90°$ (around the x axis): $(6.5, \theta, 90°, 0, 0, 0)$ which has a barrier height of 27.0 kcal/mole at $\theta = 180°$ Fig. 4(d), and rotation of the H_2O molecule around the y' axis Fig. 4(c) with a height of ~34 kcal/mole.

Shown in Figs. 5 are the rotational barriers in the neighborhood of the conformation $(6.5, 0, 90°, 180°, 0, 0)$ of Fig. 2(e), for which the (H_2O) hydrogen (NO_2^-) nitrogen distance is 2.6 Å. Among these motions, θ rotation [Fig. 5(c)] (around the x axis): $(6.5, \theta, 90°, 180°, 0, 0)$, which shows a minimum near $\theta = 60°$, is especially interesting. Here again, rotation around the dipole vector $(6.5, 0, 90°, 180°, 0, \gamma)$ [Fig. 5(a)] is almost barrier free (0.6 kcal/mole), whereas resistance to moving the dipole away from the favored direction is shown [Fig. 5(b)] to have a larger barrier of 20.8 kcal/mole.

In carrying out the SCF calculations on the above set of rotations we found another energetically favorable conformation at $(6.4, 70°, 90°, 180°, 0, 0)$ in the yz plane shown in Fig. 2(f) whose neighborhood is explored in Figs. 6. For this configuration $R_{NH} = 2.2$ Å. As is shown in Fig. 6(a), increasing $\theta(> 70°)$ involves a much "stiffer" potential increase then decreasing $\theta(< 70°)$. The results of these SCF calculations can be partly understood in terms of the scaled PCM. An increase in θ brings the (negative) O atom of H_2O closer to the O atoms of NO_2^-, thus leading to a very high barrier of 32.1 kcal/mole at $\theta = 180°$. Another interesting feature is the variation in energy accompanying variation of the angle β of the dipole vector of the H_2O molecule (rotation around the x' axis). As is shown in Fig. 6(c) the interaction potential energy goes through a small barrier of 1.9 kcal/mole at $\beta = -35°$ to end up in another local minimum at $\beta = -95°$ (which is 1.3 kcal/mole lower in energy). Although, at $\beta = 0$, $\theta = 70°$, a clockwise rotation around x' axis generally brings the H atoms closer to the O atoms of NO_2^-, the physical reason for this small barrier at $\beta = -35°$ is not entirely clear to us. Lastly we consider rotation of the H_2O around the y' axis in the neighborhood of $R = 6.5$ bohrs for conformations $(R, 150°, 0, \theta, 0, 0)$. As shown in Fig. 7, minimum energy conformations correspond to those α's that align the H atoms in toward the O atoms of NO_2^-.

The results of these rotational barrier studies can be combined with the other potential surface data mentioned earlier to see the essential aspects of the movement of an H_2O molecule in the potential field of an NO_2^- ion. Our SCF calculations show that the bonding (hydrogen-bonding) between the two molecules is essentially electrostatic with small distortions of the unperturbed orbitals of NO_2^- and H_2O. At the energetically favorable intermolecular distances, the orbitals of the fragments (NO_2^- and H_2O) show negligible mixing. Thus, one concludes that the ion–molecule forces might be adequately represented as a combination of repulsive ($\sim a\exp[-br]$), dipole–charge ($\sim \mu/R^2$), and dipole–dipole ($\sim 1/R^3$) potential functions.

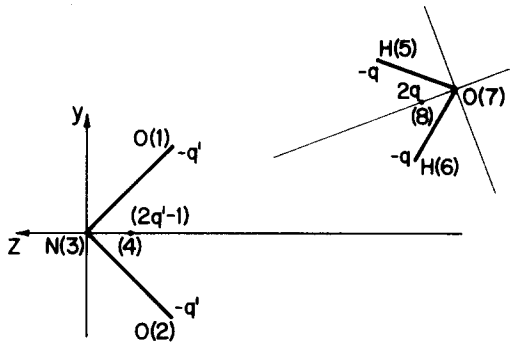

FIG. 8. Representation of the NO_2^- and H_2O molecules used in the model $NO_2^- : H_2O$ interaction potential calculations discussed in Sec. V. The indicate (4) and (8) designate the positions of the pseudoatoms (see text).

From Clementi's calculations[14] on $H_2O : H_2O$ one might estimate an average barrier of ~5 kcal/mole for a "rotation" of one water molecule in the presence of the other. Since the interactions of $NO_2^- : H_2O$ have been found to be much stronger (~17 kcal/mole), (assuming the pairwise additivity of interaction potentials) the structure of the first solvation layer of $NO_2^-(aq)$ is likely to be determined largely by these ion–dipole forces. Of course, the $H_2O : H_2O$ interactions will also play important roles in determining the orientational structure of this first hydration shell and are likely to dominate in determining the nature of the second and higher solvation layers.

V. ANALYTICAL FIT OF THE $NO_2^- : H_2O$ ENERGY SURFACE

As described in following sections, knowledge of the interaction potential between NO_2^- and H_2O is used, along with Clementi's $H_2O : H_2O$ potential,[14] to simulate the equilibrium thermodynamic of the inner hydration shells of NO_2^-. To achieve this end, we must first obtain a simple analytical expression that approximates reasonably well the above described SCF computed $NO_2^- : H_2O$ energies.

A rather simple analytical formula has been proposed by Bernal and Fowler[27] to describe the $H_2O : H_2O$ potential energy of interaction. This functional form has been successfully applied for ion : H_2O and $H_2O : H_2O$ potentials obtained from SCF and correlated calculations by Clementi *et al.*[14] and is thought to be quite reasonable for use in our case. An exponential form $A\exp(-\beta r_{ij})$ is chosen to describe the short range repulsion between pairs of atoms (labeled i, j). The long-range attractive part of the intermolecular potential is assumed to be described solely by the electrostatic interaction of the partial charges residing in the NO_2^- and H_2O fragments. Based upon the conclusions of our SCF-level calculations, it is likely that such a simple electrostatic model could accurately represent the true $NO_2^- : H_2O$ intermolecular potential hypersurface.

This model employs the following expression for the energy of $NO_2^- : H_2O$ relative to the separated fragments species, NO_2^- and H_2O [in atomic units; the atomic indices and charges are defined in Fig. 8]:

$$\Delta E(NO_2^-:H_2O) = qq'\left\{\left(\frac{1}{r_{15}}+\frac{1}{r_{16}}+\frac{1}{r_{25}}+\frac{1}{r_{26}}\right)+\frac{4}{r_{48}}-2\left(\frac{1}{r_{18}}+\frac{1}{r_{28}}+\frac{1}{r_{45}}+\frac{1}{r_{46}}\right)\right\}+q\left\{\left(\frac{1}{r_{45}}+\frac{1}{r_{46}}\right)-\frac{2}{r_{48}}\right\}+a_1\exp(-b_1r_{37})$$
$$+a_2\{\exp(-b_2r_{15})+\exp(-b_2r_{16})+\exp(-b_2r_{25})+\exp(-b_2r_{26})\}$$
$$+a_3\{\exp(-b_3r_{17})+\exp(-b_3r_{27})\}+a_4\{\exp(-b_4r_{35})+\exp(-b_4r_{36})\}$$

where a nonlinear least squares fit of our SCF-calculated energies, yields

$q=-1.169\,559$, $q'=0.620\,353$,
$a_1=2,869.9$, $a_2=2.412\,367$,
$a_3=287.2$, $a_4=5.20$,
$b_1=2.598\,981$, $b_2=1.541\,012$,
$b_3=2.454\,398$, $b_4=1.957\,793$,
$r_{34}=0.20$, $r_{78}=0.487\,741$.

The accuracy of this fit is to be judged by the values of the standard deviation and $\Delta S_K=|p_K(\partial\chi/\partial P_K)|$ (where p_K designates a parameter and χ the least squares difference) which determine the "stability" of the fit. For the 102 SCF energy points used, the standard deviation was found to be 0.000 002 a.u. The stability parameter ΔS_K was used as one of the criteria for stopping the iterative cycle. All fits were required to have $\Delta S_K \leq 10^{-6}$ for each of the parameters.

VI. MONTE CARLO SIMULATIONS OF SMALL HYDRATE CLUSTERS

Now that the SCF-level potential energy surface for the $NO_2^-:H_2O$ dimer has been characterized analytically for thermally accessible regions of molecular conformation space, we are prepared to undertake the Monte Carlo simulation aspect of this research. In order to study the patterns of distribution of water molecules around the nitrite ion, we also need to know the interaction potential between pairs of water molecules. As mentioned earlier, we chose to use the water dimer potential surface calculated by Clementi *et al.*[14] These authors have found the "linear," the "bifureated" and the "cyclic" conformations to be among the more stable arrangements, giving binding energies of 5.6, 4.9, and 4.2 kcal/mole, respectively. Qualitatively speaking, these conformations have geometrical characteristics which bring the H and O atoms of two neighboring water molecules close while keeping the H–H and O–O distances large. For a more complete description of the $H_2O:{}_2HO$ dimer surface as well as the analytic representation of this surface introduced by Clementi *et al.*, see Ref. 14.

A. Theoretical Background and the Monte Carlo procedure

We have employed the Monte Carlo (MC) procedure of Metropolis *et al.*[28] to study the equilibrium thermal distribution of various $NO_2^-:(H_2O)_n$ clusters. In this procedure a Markov Chain is constructed with transition elements p_{ij} connecting two states i and j (conformations: $R, \theta, \phi, \alpha, \beta, \nu$), whose limit distribution $\{\pi_i\}$ is the thermal equilibrium distribution ($\{e^{-E_i/kT}\}$). The transition elements p_{ij} are defined in terms of the underlying symmetric Markov Chain (stream of Random numbers for example) elements p_{ij}^* as

$$p_{ij}=\begin{cases} p_{ij}^* & \pi_j \geq \pi_i,\ j\neq i \\ p_{ij}^*\,\pi_j/\pi_i & \pi_j<\pi_i;\ j\neq i \end{cases}$$

$$\sum_j p_{ij}=1\ .$$

The average of a quantity A, taken over the successive states of this Markov Chain approaches the (thermal) average over the desired limiting distribution as $t^{-1/2}$.

$$\bar{A}_t \equiv \frac{1}{t}\sum_i A(q_i)=\sum_{q\in\Gamma}A(q)\pi(q)+\mathcal{O}(t^{-1/2})=\langle A\rangle+\mathcal{O}(t^{-1/2})\ ,$$

where t is the number of steps in the chain. Here $q\in\Gamma$ designates conformational points q that lie within the physical boundaries prescribed by the molecular geometries involved.

For the cases under study, given the initial state (i) of the $NO_2^-:(H_2O)_n$ cluster described by the conformations of the n water molecules, the equilibrium distribution of these water molecules was achieved as follows:

i) Using a stream of random numbers, one of the n H_2O molecules is picked, and a displacement of one of its six degrees of freedom is chosen, thereby giving a new state j. This displacement involves changes either in one of the Cartesian coordinates δ_x, δ_y, or δ_z of the O atom uniformly distributed on $(-\Delta, \Delta)$ or in an orientational angle α, β, or γ uniformly distributed on $(-\psi, \psi)$. The step lengths Δ and ψ were chosen to give approximately 60% acceptance of the MC passes.

ii) The change in the cluster's potential energy $\Delta E(=E_j-E_i)$ for the above displacement is calculated in a pairwise additive approximation using the SCF-level $NO_2^-:H_2O$ surface and Clementi's $H_2O:H_2O$ surface.

iii) If the energy change ΔE is negative ($\pi_j \geq \pi_i$) the move is accepted. If ΔE is positive ($\pi_j<\pi_i$) the move is accepted with a probability equal to $\pi_j/\pi_i=\exp(-\Delta E/kT)$ and rejected with probability $1-\exp(-\Delta E/kT)$. This last step is accomplished by comparing $\exp(-\Delta E/kT)$ with a random number x uniformly distributed on (0, 1); if $\exp(-\Delta E/kT)>x$ the move is accepted, otherwise it is rejected.

Repeated application of these rules to the conformational points of the cluster $NO_2^-:(H_2O)_n$ ensure that the sampling approaches the thermal Boltzmann (limit) distribution. As in all such applications of MC procedures, one is faced with making "good" choices for the "initial" conformation of the cluster under study. Our approach to this problem is as follows: Starting from a more-or-

less arbitrarily chosen initial conformation of the cluster the system was "matured" at $T = 4\,^\circ K$ through $\sim 2 \times 10^4$ MC passes in order to allow the H_2O molecules to move to relatively low energy positions. This "system initialization" was then followed by $\sim 5 \times 10^4$ MC passes at $T = 300\,^\circ K$ to ensure that the system had reached thermal equilibrium. These initial (5×10^4) conformations were then discarded to avoid dependence of computed thermal averages on the starting conformation. Unless otherwise stated, all of the results reported below involving statistical averages were then obtained by averaging over the next (at least) 2.5×10^5 MC passes. The assumption that the above "maturing" procedure was successful was checked by repeating the entire process at a different (input) initial conformation and drawing, for each initial conformation, the distributions of cluster interaction energies which display some dispersion around a peak average (equilibrium) value. Such energy distribution graphs were found to be indistinguishable for the various starting points. The structures of the individual cluster $NO_2^-(H_2O)_n$ $n = 1, \ldots, 16$, some of which are discussed below, were built up by performing separate MC calculations for each of these clusters. To analyze in detail the "shapes" of these clusters we have calculated the R distribution functions with a grid size of 0.1 bohr, the θ distribution function over 5° increments, the (R, θ) distribution and the cluster energy (E) in a 0.2 hartree neighborhood of the most probable energy. The θ distribution function, for example, gives the probability of finding any water molecule (from among the n such molecules) within θ and $\theta + \Delta\theta$ irrespective of α, β, γ, R, and ϕ.

B. Structure of clusters

The relevance of the small cluster sizes considered here to the bulk behavior of NO_2^-(aq) is, of course, not obvious. In systems with long range (ion–dipole, dipole–dipole) forces, one can not hope to achieve an adequate estimation of the *thermodynamic properties* (heat capacities, entropies, internal pressure, etc.) through such small cluster investigations. However, we are not interested in such bulk properties. We want to probe the "shape" of the inner hydration shells in NO_2^-(aq) because it is (presumably) these inner shells which have dominant effects upon the position and in-

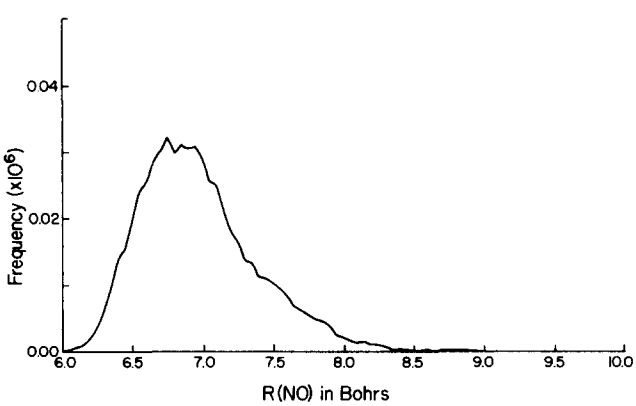

FIG. 9. R distribution function for $n = 3$.

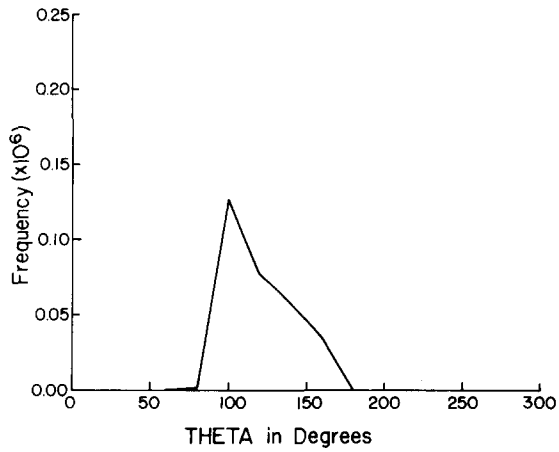

FIG. 10 θ distribution function for $n = 3$.

homogeneous width of the $n\pi^*$ electronic absorption in this system.[4] Therefore, our studies of the smaller $NO_2^- : (H_2O)_n$ clusters must be viewed as involving prototype systems which could simulate the equilibrium behavior of $NO_2^-(H_2O)_n$ in equilibrium with a surrounding which could either be other H_2O solvent molecules or some other "solvent" species. For these reasons, it is not at all clear that our results for $NO_2^-(H_2O)_n$ relate to what is expected to occur in small *isolated* clusters such as are formed in nozzles or beams.

In light of these qualifications we can now proceed to examine the patterns in which distribution of water molecules around the nitrite ion, as we progressively build up the "first hydration layer" of NO_2^-. Because the $NO_2^- : H_2O$ interactions energy (~17 kcal/mole) is much stronger than the $H_2O : H_2O$ energy (~5 kcal/mole), the distribution of water molecules around the ion within the first hydration layer would be expected to be largely determined by the $NO_2^- : H_2O$ interaction. However, beyond the first layer, where the ion–water distances are $\lesssim 10$ bohrs (the $NO_2^- : H_2O$ minimum energy conformations are at 6.2–7 bohrs and the optimum $H_2O : H_2O$ distances are at 4–5 bohrs), the ion–water and water–water interactions are of similar magnitude. In addition, the electrostatic potential around the NO_2^- ion is certainly not spherically symmetric and hence we expect the distribution of the H_2O molecules to reflect this behavior. As we shall discuss in more detail below, one consequence of this anisotropic potential is that a second hydration shell (as defined by the R and θ values of the participating H_2O molecules) begins at $n = 6$ although all of the six water molecules are contained in the $\theta > 90°$ hemisphere. Although the anisotropy eventually gives way to allow NO_2^- to be entirely surrounded by H_2O molecules in the aqueous system, it is likely that for such smaller clusters, which can be "grown" in nozzle expansion experiments, the angular distribution of the H_2O molecules is highly nonspherical.

The MC simulations for cluster sizes $n \leq 5$ show that the H_2O molecules are distributed inside the $\theta > 90°$ hemisphere around the nitrite ion. Figures 9 and 10 display the R and θ distributions for $n = 3$ and Figs. 11 and 12 do likewise for $n = 5$. These R distributions are near-

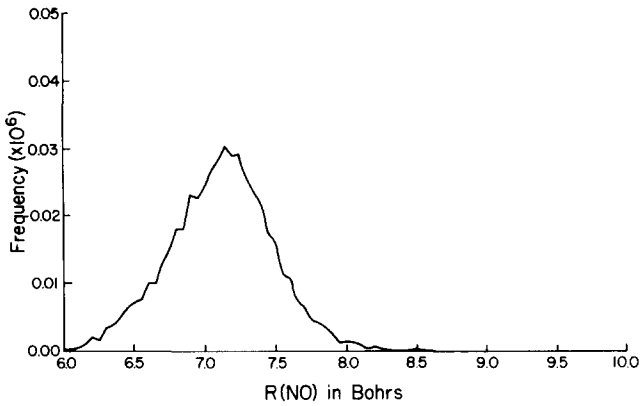

FIG. 11. R distribution function for $n=5$.

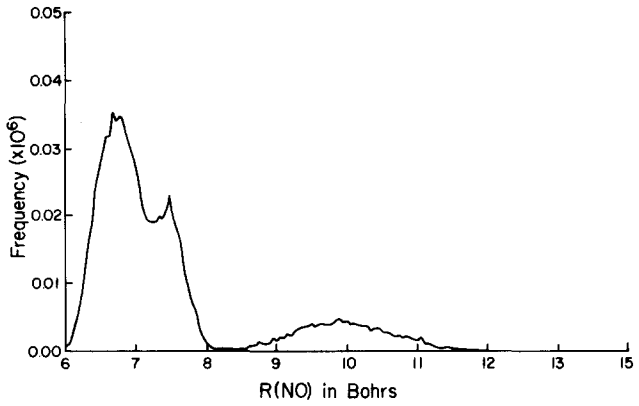

FIG. 13. R distribution function for $n=6$.

ly structureless and have maxima at $R=6.7$ bohrs for $n=3$ and at $R=7.0$ bohrs for $n=5$, thereby showing a small shift to larger R for increasing n. Elementary geometrical considerations show that, on the surface of a hemisphere of radius 7 bohrs, five water molecules can be easily accommodated (i.e., having O–O distances of at least 5 bohrs). Thus, there exists much radial and orientational flexibility (since there are numerous low energy conformations in the $\theta > 90°$ hemisphere) which gives rise to a smooth shape in the resulting R distribution functions. Moreover, it is quite likely that, in going from $n=1$ to $n=5$, the repulsive water–water interactions give rise to a small increase in the most probable R values and to θ distribution functions which show an increasing probability at lower θ values. These are simply "packing" effects.

Once the cluster size reaches $n=6$, we notice a new behavior in which there exists a definite probability of finding water molecules at $R \sim 10$ bohrs and $\theta > 90°$ as well as a continuation of the above described trends toward larger R and smaller θ for the remaining H_2O molecules. The R, θ, E, and (R,θ) distributions functions for $n=6$ are shown in Figs. 13, 14, 15, and 16, respectively. An important question suggested by these results concerns why conformations at $R \sim 10$ bohrs having large θ are preferable to those at $R \sim 6.5$ bohrs at smaller θ values, even though the $NO_2^-:H_2O$ pair potential at $\theta=0$, $\phi=0$, $R=6.5$ bohrs is about 5.5 kcal/mole lower in energy than at $R=10$, $\theta=180$, $\phi=0$. To make sure that this observation is not an artifact of the choice of initial MC conformation, calculations were performed with other initial conformations, the results of which did indeed verify the existence of finite probability at $R \sim 10$ bohr. To further examine this behavior we monitored the interaction energies over 100 MC passes, of a special $n=6$ cluster in which a "tagged" molecule was *fixed* at (6.5, 0°, 0°, 0°, 0°, 0) with the ion (fixed) and the remaining five water molecules in *thermal equilibrium* with this tagged molecule. These results were compared with the actual $n=6$ (no constraint) distribution of Figs. 13 to 16. A comparison of the interaction energies shows that, although the NO_2^- interaction energies for the tagged molecule are indeed lower by 3–5 kcal/mole over that at $R \sim 10$ bohr, $\theta > 90°$, the water–water interactions energies involving the tagged H_2O and the remaining five H_2O's are nearly always unfavorable enough to make the conformations with a water molecule at $R \sim 10$, $\theta > 90°$ energetically favorable. As a matter of fact, the net water–water interaction on the tagged molecule was found to be repulsive. This is because the tagged molecule essentially "faces" the remaining five H_2O's. For another $n=6$ cluster, in which the tagged H_2O molecule

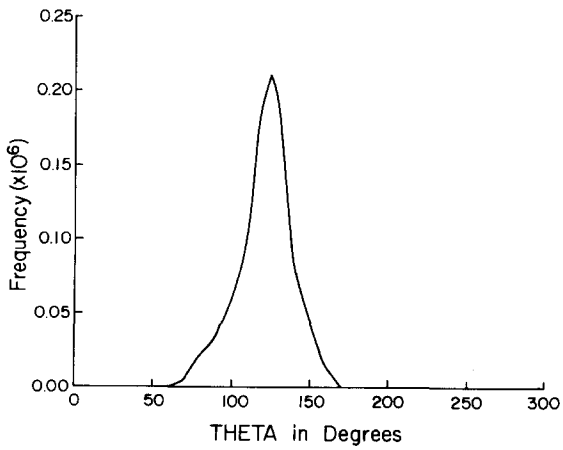

FIG. 12. θ distribution function for $n=5$.

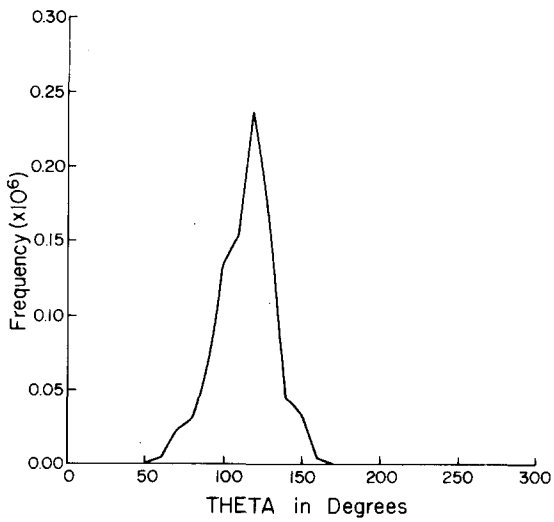

FIG. 14. θ distribution function for $n=6$.

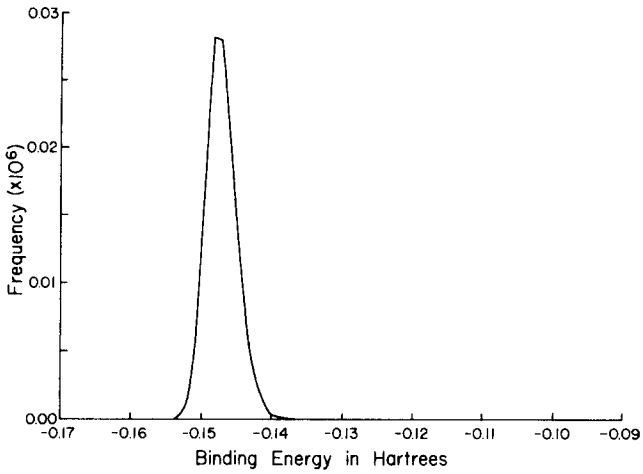

FIG. 15. Distribution function of the total binding energy for $n=6$.

was fixed at (6.5, 70°, 90°, 180°, 0, 0), it is found that the interaction energies compare well (within 0.2 to 0.4 kcal/mole) with the actual $n=6$ cluster. This analysis, of course, involves only a few selected conformations and thus is decidedly incomplete. However we hope that it gives some understanding of the distribution of water molecules in the $n=6$ cluster.

The distinguishing features of the larger clusters ($n \geq 6$) are

i) that the second hydration layer (defined as those H_2O's having $R>9$ bohrs) involves progressively more H_2O molecules,

ii) with increasing n, the radial (R) structure in the first hydration layer becomes more pronounced, whereas its "peak" value remains almost constant,

iii) there is a trend for the θ distribution to shift toward smaller θ values as n increases,

iv) once $n=14$–15, the NO_2^- ion is "surrounded" by at least one layer of water molecules.

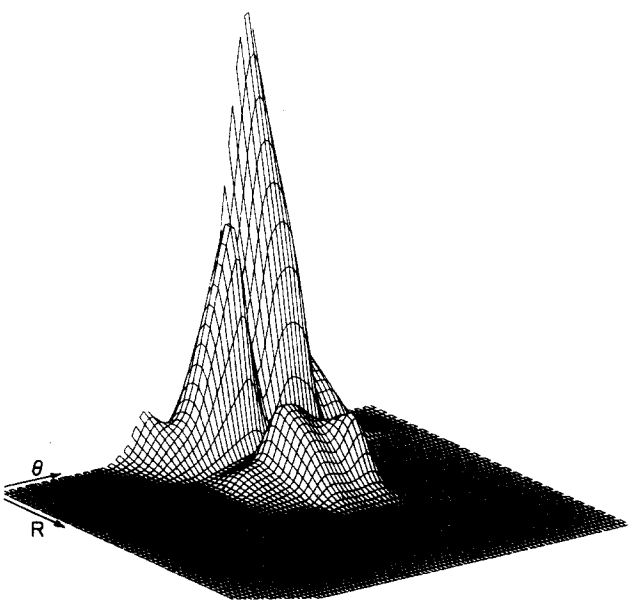

FIG. 16. (R, θ) distribution function for $n=6$, for $6.0 \leq R \leq 16.5$ bohrs and $0 \leq \theta \leq \pi$ radians represented on orthogonal Cartesian axes.

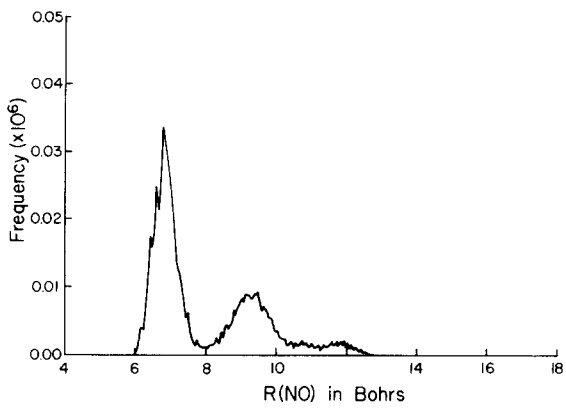

FIG. 17. R distribution function for $n=9$.

The R and θ distributions for $n=9$ are shown in Figs. 17 and 18, and the R, θ, E, and (R, θ) distributions for $n=15$ are shown in Figs. 19, 20, 21, and 22, respectively. The kind of trends mentioned above can be partially explained based upon the results of the "tagged" molecule experiment for $n=6$ discussed above. In going from $n=6$ to $n=7$, for example, the added molecules are likely to go to either of two "locations": toward lower θ values in the first layer or to the second layer (which has slightly larger probability). The distribution functions for $n=9$ given in Figs. 17 and 18 show the occurrence of these two processes. The more pronounced structure in the radial distribution of the first hydration layer can be attributed a "steric" effect. Being enveloped by the $R=10$ bohr layer, the movements of the water molecules in the first hydration layer are significantly restricted both by the surrounding H_2O's as well as by the NO_2^-. This restricted motion is in contrast to situations arising for the clusters $n=1, \ldots, 5$ where large geometrical variations occur. From $n=15$ cluster calculations we estimate that there are 7 to 8 water molecules in the first hydration layer around NO_2^-.

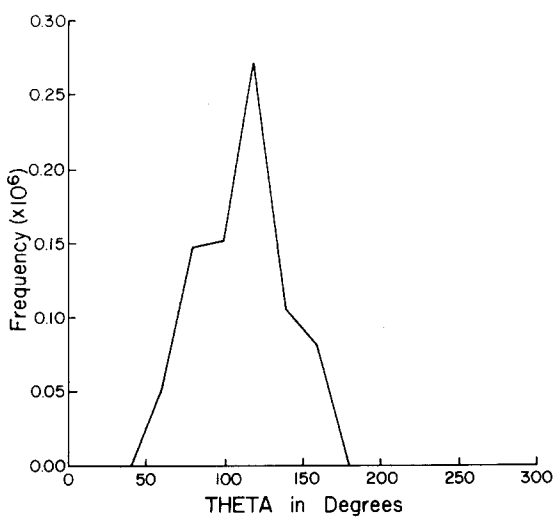

FIG. 18. θ distribution function for $n=9$.

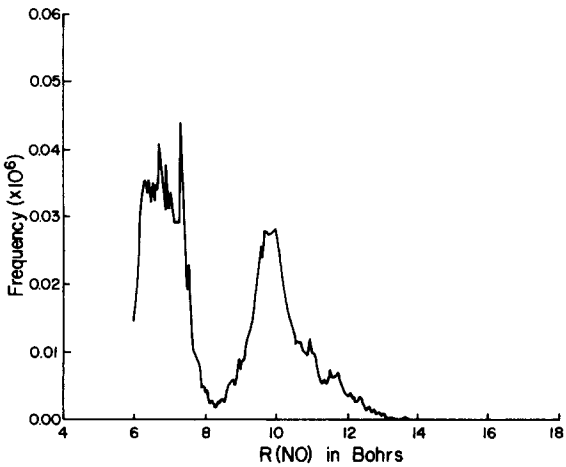

FIG. 19. R distribution function for $n = 15$.

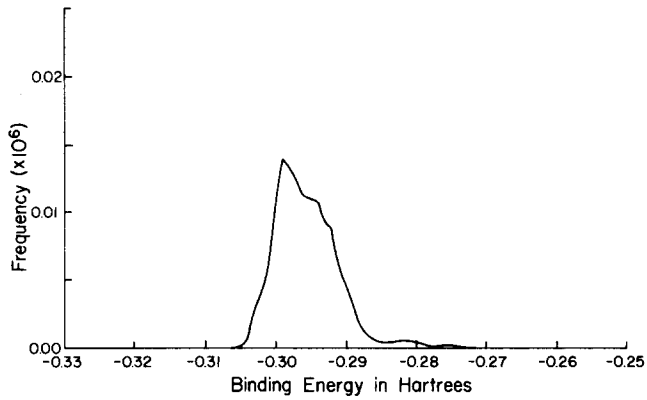

FIG. 21. Distribution function of the total binding energy for $n = 15$.

The (R, θ) distribution for $n = 15$ given in Fig. 22 shows additional details of the structure caused by the anisotropy and strengths of the electrostatic potential around NO_2^- and by the "steric" effects among the water molecules. To further probe the "strengths" of this structure, we performed another MC calculation for $n = 15$ at $T = 500\,^\circ$K. In this situation we expect increased movement of the water molecules because conformations of higher energy (10 kcal/mole $= 10\,KT$ and $T = 500\,^\circ$K) are now thermally accessable. The results of these higher temperature MC calculations yield an R distribution which shows the same basic structure as for $T = 300\,^\circ$K even though the distribution is broader, as expected.

To indicate the behavior of the average total energy (computed as a pairwise sum) as a function of the cluster size (E_n), we display in Fig. 23 the energy increments $\Delta E_n = E_n - E_{n+1}$ vs n. In the limit of large n, where the results must simulate the NO_2^- (aqueous) solution, we expect the slope ($\lim_{n\to\infty} \Delta E_n$) to tend toward a constant value since ΔE_n corresponds to the energy required to pull the $(n+1)$th water molecule away from the $NO_2^- : (H_2O)_n$ core. Clearly as can be seen from Fig. 23, we have not reached this limiting case. The simulation of NO_2^- : (aqueous) will require larger clusters because of the long range ion–dipole and dipole–dipole interactions that are involved. However, we again emphasize that our aim is not to study such bulk behavior but rather to have enough H_2O molecules surrounding the NO_2^- such that the electronic excitation ($n\pi^*$) energy of the NO_2^- is insensitive to addition to another H_2O.

VII. CONCLUDING REMARKS

We have presented the results of *ab initio* SCF-level calculations at 102 intermolecular conformations of $NO_2^- : H_2O$. These calculations were performed using the MOLECULE integral package[29] and the GRNFNC[30] SCF computer programs, on the University of Utah DEC-20 computer. We have carried out Monte Carlo simulations of the hydration structure of several small clusters, $NO_2^- : (H_2O)_n$, $n = 1$ to 16. Our next goal is to use these

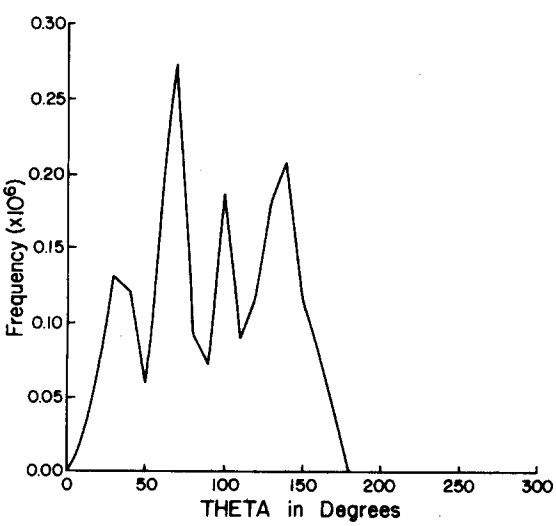

FIG. 20. θ distribution function for $n = 15$.

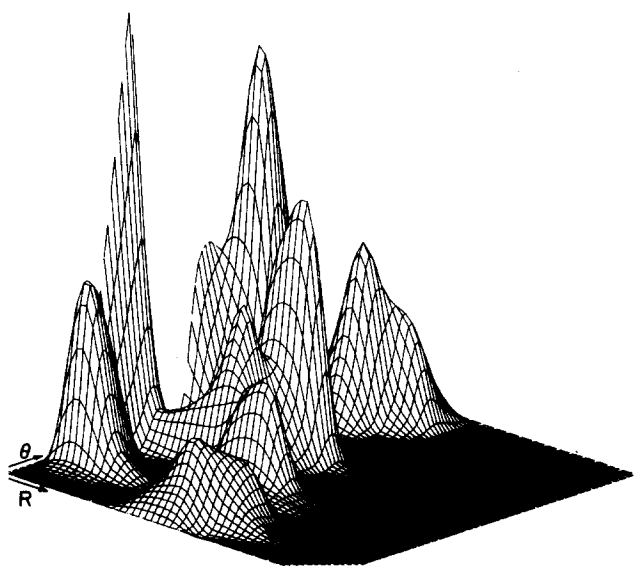

FIG. 22. (R, θ) distribution function for $n = 15$, for $6.0 \leq R \leq 16.5$ bohrs and $0 \leq \theta \geq \pi$ radians represented on orthogonal Cartesian axes.

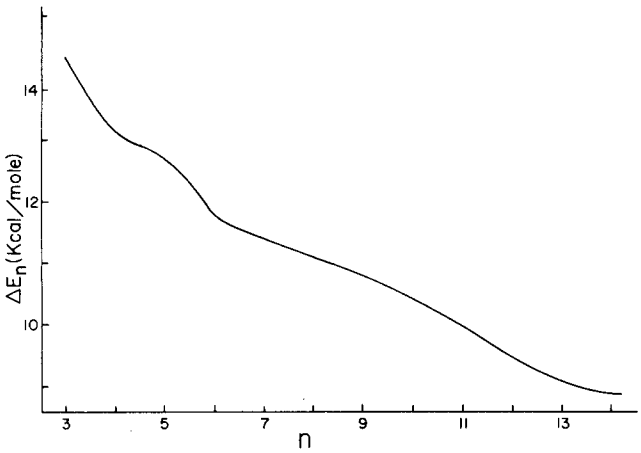

FIG. 23. Behavior of total energy differences $\Delta E_n = E_n - E_{n+1}$ (kcal/mole) as a function of the cluster size, n.

results, which tell us how H_2O molecules "pack" around an NO_2^- ion, along with results of our CI calculations on the first ($n\pi^*$) excited state of $NO_2^-:H_2O$ to perform Monte Carlo calculations aimed at elucidating the spectroscopic properties such as the band maximum, and inhomogeneous broadening of the $n\pi^*$ absorption.

ACKNOWLEDGMENTS

The authors acknowledge support from the National Science Foundation (Grant #CHE78-09734), and for support of the Utah DEC-20 computer facility.

[1]A. Good, D. A. Durden, and P. Kebarle, J. Chem. Phys. **52**, 212, 222 (1970); E. E. Ferguson and F. C. Fehsenfeld, J. Geophys. Res. **14**, 5743 (1969).
[2]P. Kebarle, S. K. Searles, A. Zolla, J. Searborough, and Arshadi, J. Am. Chem. Soc. **89**, 6393 (1967).
[3]*Electron–Solvent and Anion–Solvent Interactions*, edited by L. Kevan and B. C. Webster (Elsevier, Amsterdam, 1976); *Advances in Radiation Chemistry*, edited by E. T. Kaiser and L. Kevan (Wiley, New York, 1974), Vol. 4; Can. J. Chem. **55**, (1977); *Radiation Research: Biomedical, Chemical, and Physical Perspectives*, edited by O. F. Nygaard, H. I. Adler, and W. K. Sinclair (Academic, New York, 1975); Proc. 5th Int. Cong. Rad. Res., Seattle, 1974; *Electrons in Fluids*, edited by J. Jortner and N. R. Kestner (Springer, New York, 1973).
[4]A. Banerjee and J. Simons, J. Chem. Phys. **68**, 415 (1978); J. Simons, Int. J. Quantum Chem. **13**, 553 (1978); J. McHale, A. Banerjee, and J. Simons, J. Chem. Phys. **69**, 1406 (1978), A. Banerjee and J. Simons, J. Chem. Phys. **69**, 5538 (1978); A. Banerjee and J. Simons, J. Chem. Phys. **71**, 60 (1979).
[5]J. McHale and J. Simons, J. Chem. Phys. **67**, 389 (1977); **68**, 1695 (1978).
[6]R. A. Ogg, J. Am. Chem. Soc. **68**, 155 (1946); J. Chem. Phys. **14**, 114, 295 (1946); Phys. Rev. **69**, 243, 668 (1946).
[7]W. N. Lipscomb, J. Chem. Phys. **21**, 52 (1953).
[8]R. A. Stairs, J. Chem. Phys. **27**, 1431 (1957).
[9]J. Jortner, J. Chem. Phys. **30**, 839 (1957).
[10]M. Weissmann and N. V. Cohan, Chem. Phys. Lett. **7**, 445 (1970); J. Chem. Phys. **59**, 1385 (1973); M. Tachiya and A. Mozumder, J. Chem. Phys. **60**, 3037 (1974); **61**, 3690 (1974); C. A. Naleway and M. E. Schwartz, J. Phys. Chem. **76**, 3905 (1972); M. D. Newton, J. Chem. Phys. **58**, 5833; B. Webster, J. Phys. Chem. **79**, 2809 (1975).
[11]M. Tachiya, J. Chem. Phys. **60**, 2275 (1974); J. T. Waber and D. A. Liberman, J. Chem. Phys. **57**, 967 (1972).
[12]J. Jortner, J. Chem. Phys. **30**, 839 (1959); D. A. Copeland, N. R. Kestner, and J. Jortner, J. Chem. Phys. **53**, 1189 (1970); K. Fucki, D. F. Feng, and L. Kevan, J. Am. Chem. Soc. **95**, 1398 (1973).
[13]M. D. Newton, J. Phys. Chem. **79**, 2795 (1975); M. D. Newton and S. Ehrenson, J. Am. Chem. Soc. **93**, 4971 (1971).
[14]E. Clementi and H. Popkie, J. Chem. Phys. **57**, 1077 (1972); H. Kistenmacher, H. Popkie, and E. Clementi, J. Chem. Phys. **58**, 5627 (1973); J. Chem. Phys. **59**, 5627 (1973); J. Chem. Phys. **61**, 799 (1974), O. Matsuoka, E. Clementi, and M. Yoshimine, J. Chem. Phys. **64**, 1351 (1976); G. Bolis and E. Clementi, J. Am. Chem. Soc. **99**, 5550 (1977); R. O. Watts, E. Clementi, and J. Fromm, J. Chem. Phys. **61**, 2 2550 (1974); R. Scordamaglia, F. Cavallone, and E. Clementi, J. Am. Chem. Soc. **99**, 5545 (1977).
[15]A. Pullman, B. Pullman, and H. Berthod, Theoret. Chim. Acta **47**, 175 (1978); A. Pullman, H. Berthod, and N. Gresh, Theoret. Chim. Acta **40**, 47, 71, 93 (1975); B. Pullman, N. Gresh, H. Berthod, and A. Pullman, Theoret. Chim. Acta **44**, 151 (1977); Int. J. Quant. Chem. Symp. **10**, 59 (1976); Theoret. Chim. Acta **33**, 11 (1975); A. Pullman in: *The World of Quantum Chemistry*, Proceedings of the First International Congress, Menton, France (1973).
[16]P. A. Kollman and L. C. Allen, J. Am. Chem. Soc. **93**, 4991 (1971).
[17]S. Swaminathan, S. W. Harrison, and D. L. Beveridge, J. Am. Chem. Soc. **78**, 5705 (1978).
[18]G. H. F. Diereksen, W. P. Kraemer, and B. O. Ross, Theoret. Chim. Acta **36**, 249 (1975).
[19]J. O. Noell and K. Morokuma, Chem. Phys. Lett. **36**, 465 (1975); J. Phys. Chem. **80**, 2675 (1976);
[20]T. H. Dunning, J. Chem. Phys. **53**, 2823 (1970).
[21]S. Huzinaga, J. Chem. Phys. **42**, 1293 (1965).
[22]J. Simons, Int. J. Quant. Chem. **11**, 971 (1977); *Theoretical Chemistry: Advances and Perspectives*, H. Eyring and D. Henderson, Editors (Academic, New York, 1977).
[23]R. Bonaccorsi, C. Petrongolo, E. Scrocco, and J. Tomasi, J. Chem. Phys. **48**, 1497 (1968).
[24]P. Benioff, J. Chem. Phys. **68**, 3405 (1978).
[25]R. Ditchfield, W. Hehre, and J. A. Pople, J. Chem. Phys. **54**, 724 (1971).
[26]G. G. Hall, Chem. Phys. Lett. **20**, 501 (1973).
[27]J. D. Bernal and F. D. Fowler, J. Chem. Phys. **1**, 515 (1933).
[28]N. Metropolis, A. W. Metropolis, M. N. Rosenbluth, A. H. Teller, and E. Teller, J. Chem. Phys. **21**, 1087 (1953).
[29]J. Almlöf, Report 74-29 (Dec. 1974), Report 72-09 (Sept. 1972), Institute of Physics, University of Stockholm.
[30]G. Purvis, Battelle Memorial Institute, Columbus, Ohio.